

# Aharonov-Bohm effect for the edge states of zigzag carbon nanotubes

K. Sasaki,\* M. Suzuki, and R. Saito

*Department of Physics, Tohoku University and CREST, JST, Sendai 980-8578, Japan*

(Dated: November 30, 2018)

Two delocalized states of metallic zigzag carbon nanotubes near the Dirac point can be localized by the Aharonov-Bohm magnetic field around 20 Tesla. The dependence of the localization on the length and diameter of the nanotubes shows that the localization-delocalization transition can be observed for 2 nm diameter tube. The mechanism of the localization is explained in terms of the deformation-induced gauge field, which shows a topological nature of the localization. The transition from the delocalized states to the localized states can be observed by scanning tunneling microscopy and spectroscopy. A similarity between the transition and the spin Hall effect is discussed.

## I. INTRODUCTION

The electronic properties of graphene have attracted much attention from various points of view. It is found that graphene shows the integer quantum Hall effect<sup>1,2</sup> and dissipationless supercurrent.<sup>3</sup> These effects are attributed to the energy band structure of graphene which consists of two Dirac cones at the K and K' points in the  $k$ -space. The dynamics of electrons around each Dirac point is approximated by the Weyl equation, which describes a “massless” particle. The “massless” particle never stop and the wave function is generally extended. However, electrons can be localized near the zigzag edge of graphene, which are called the edge states.<sup>4</sup> The appearance of the edge states is sensitive to the shape of the edge, that is, the zigzag edge induces the edge states while the armchair edge does not. Since the energy dispersion of the edge states as a function of the wave vector along the edge direction appears near the Dirac points, the local electronic properties such as ferromagnetism<sup>4</sup> and superconductivity<sup>5</sup> near the zigzag edge are proposed in terms of the edge states. The edge states exist near the zigzag end of a single-wall carbon nanotube, too, because a carbon nanotube is a graphene sheet wrapped into a cylinder.

The energy dispersion relation of the zigzag edge states appears only between the two Dirac points, and the localization length ( $\xi$ ) of the edge state depends on the distance from the Dirac point in the  $k$ -space. In particular, at the center of the two Dirac points, the wave function of the edge state has amplitude only at the edge sites ( $\xi = 0$ ). While  $\xi$  becomes infinite at the Dirac points where the edge states connect to extended states continuously. Thus, by changing  $k$  due to the Aharonov-Bohm (AB) effect for the magnetic flux penetrating a hollow core of nanotube,<sup>6</sup> an extended state at the Dirac point can be transferred into an edge state and vice versa (localization-delocalization (LD) transition). In the previous paper,<sup>7</sup> we showed that the LD transition is possible for large diameter zigzag nanotubes and it can be observed by the conductance measurement. In this paper, we first show analytical calculations of the length and diameter dependence of the LD transition, and then try to explain the phenomena intuitively using a contin-

uous model. We will show that the LD transition can be observed by scanning tunneling microscopy (STM) and spectroscopy (STS) measurements in the presence of magnetic field around 20 Tesla.

Since the edge states exist near the Fermi energy, the real-space image of the edge states is observed by STM experiments.<sup>8,9,10,11,12,13</sup> The local density of state (LDOS) is observed by STS at a step edge of the zigzag type on a vicinal surface of graphite.<sup>8,9,11,12,13</sup> The cylindrical structure of carbon nanotubes is suitable for the study of the AB effect. The AB oscillations and the period of the fundamental unit of magnetic flux ( $\Phi_0$ ) were observed in multi-wall nanotubes.<sup>14,15</sup> Since AB flux breaks time-reversal symmetry, a splitting of the degenerated van Hove singularity for K and K' points is observed.<sup>6,16,17</sup> The splitting was observed as a shift of the first-subband magneto-absorption peak in semiconducting single-wall nanotubes<sup>18</sup> and as a splitting of the peak position of the van Hove singularities in the conductance measurement.<sup>19</sup> These experiments are intended to observe the AB effect for the extended states near the Fermi level. The AB measurement by STM/STS for the edge states not only gives a direct evidence of the edge states in zigzag carbon nanotubes but also can clarify the topological property of the edge states.

An important property of the edge state is that the wave function of the edge state has an amplitude only on one of the two sublattices (A and B) in the hexagonal lattice. When we consider a pseudo 1/2 spin whose up and down spins represent the relative amplitude on the A and B sublattices, respectively, an edge state can be described by a pseudo-spin polarized state accumulated at the edge. This situation is similar to the spin Hall effect<sup>20,21,22</sup> in which the spin-orbit interaction induces the spin polarization at the edge of semiconductor materials by “the Lorentz force for spin” in the presence of the electronic current. In this paper, we will show that a similar Lorentz force acts for the pseudo spin in the graphene system in which the lattice defects can be understood by the time-reversal-symmetric gauge field and by corresponding pseudo-magnetic field.

In Sec. II, we show the AB effect for the edge states. In Sec. III, the pseudo spin and corresponding Hamiltonian are defined and the Lorentz force for the pseudo spin is derived. In Sec. IV, discussion and summary will be

given.

## II. AB EFFECT FOR THE EDGE STATES

Here, we define the wave number around and along the axis of a tube as  $k_c$  and  $k_t$ , respectively. Because of the periodic boundary condition around the axis for a  $(n, 0)$  zigzag nanotube,  $k_c$  is discrete as  $k_c = 2\pi p/|\mathbf{C}_h|$  ( $p$  is integer) where  $|\mathbf{C}_h| = na$  and  $a = 0.246$  nm is the lattice constant.  $k_t$  is also quantized by the boundary condition in the direction of the axis of the tube for a finite length  $L$ . In the previous paper,<sup>7</sup> we give the boundary condition for  $k_t$  as follows,

$$-2 \left(1 + \frac{\alpha}{n^2}\right) \cos\left(\frac{k_c a}{2}\right) = \frac{\sin(k_t(L + \ell))}{\sin(k_t(L + 2\ell))}, \quad (1)$$

where  $2\ell \equiv \sqrt{3}a$  is the unit length in the direction of the axis and  $\alpha$  is a parameter representing the curvature effect. The energy for  $\pi$ -band is given by

$$E(k_c, k_t) = \pm\gamma_0 \sqrt{g(k_c)^2 + 2g(k_c) \cos(k_t \ell) + 1}, \quad (2)$$

$$\text{where } g(k_c) \equiv 2 \left(1 + \frac{\alpha}{n^2}\right) \cos\left(\frac{k_c a}{2}\right)$$

and  $\gamma_0$  ( $\approx 3$  eV) is the nearest neighbor hopping integral.

First we consider the case of  $\alpha = 0$  in Eqs. (1) and (2) for simplicity. Then we will discuss the case for  $\alpha = \pi^2/8$  which is derived previously.<sup>7</sup> For the K point  $(k_c, k_t) = (4\pi/3a, 0)$  (K' point  $(k_c, k_t) = (2\pi/3a, \pi/\ell)$ ), we get  $g(k_c) = -1$  ( $g(k_c) = 1$ ) and  $E(k_c, k_t) = 0$  (Dirac points).

Depending on the value of  $k_c$ , Eq. (1) has real and imaginary solutions for  $k_t$  corresponding to the extended and the edge states, respectively. It can be shown that the edge states appear when  $2\pi/3a < k_c < 4\pi/3a$  ( $|g(k_c)| < 1$ ), and that  $k_t$  for the edge state satisfies

$$k_t = \begin{cases} \frac{\pi}{\ell} + \frac{i}{\xi(k_c)} & \left(\frac{2\pi}{3a} < k_c < \frac{\pi}{a}\right) \\ \frac{i}{\xi(k_c)} & \left(\frac{\pi}{a} < k_c < \frac{4\pi}{3a}\right) \end{cases} \quad (3)$$

where  $\xi(k_c)$  denotes the localization length of the edge state defined by  $\xi(k_c) = -\ell/\ln(|g(k_c)|)$ .<sup>7</sup> At  $k_t = 0$  or  $\pi/\ell$  (or when  $\xi(k_c)$  becomes  $\infty$ ), we have a discontinuous change of  $k_t$  (see Fig. 1(a)). The states for  $k_t = 0$  or  $k_t = \pi/\ell$  can be called ‘‘critical states’’ since they can be regarded both as an extended state ( $k_t$  is a real number) and as a localized state with infinite localization length ( $\xi \rightarrow \infty$ ). By substituting  $k_t = 0$  into Eq. (1), we obtain

$$\begin{aligned} k_c^{\text{critical}} &= \frac{2}{a} \arccos\left(-\frac{1}{2} \frac{L + \ell}{L + 2\ell}\right) \\ &\approx \frac{4\pi}{3a} - \frac{1}{L}, \quad (L \gg \ell). \end{aligned} \quad (4)$$

$k_c^{\text{critical}}$  corresponds to the K point ( $g(k_c^{\text{critical}}) = -1$ ) when  $L \rightarrow \infty$ . Similarly,  $k_t = \pi/\ell$  gives  $k_c^{\text{critical}} \approx 2\pi/3a + 1/L$  ( $L \gg \ell$ ) and  $k_c$  becomes the K' point in the limit of  $L \rightarrow \infty$ . In Fig. 1(b), we plot Eq. (2) around the K point as a function of  $k_c$  where  $k_t$  is determined by Eq. (1).  $k_t$  is a real number in the shaded region while  $k_t$  is a complex number outside of the shaded region (localized region). The critical states are denoted by the solid black circles. For the critical states, we obtain  $g(k_c^{\text{critical}}) \approx -1 + \ell/L$ . By putting this into Eq. (2), we obtain the energy eigenvalues of the critical states as  $E(k_c^{\text{critical}}, 0) = \pm\gamma_0 \ell/L$ . The critical states are located on the intersection made by the surface of the Dirac cone and the plane of  $k_t = 0$ . The intersection is denoted by the dashed lines in Fig. 1(b).

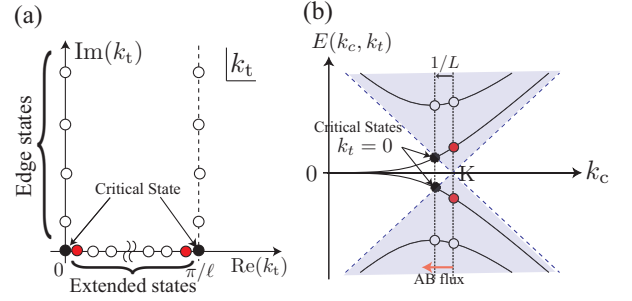


FIG. 1: (color online) (a) In the complex plane of  $k_t$ , the extended states have real  $k_t$ , while the edge states have imaginary part in  $k_t$ .  $k_t = 0$  (and  $k_t = \pi/\ell$ ) is the critical state. (b) The energy band structure  $E(k_c, k_t)$  near the K-point is plotted as a function of  $k_c$  where the  $k_t$  axis is perpendicular to the plane. Each dispersion curve corresponds to a different value of  $k_t$ . The two states represented by the red circles can go out of the surface of the Dirac cones at the critical states (represented by solid black circles) by means of the AB flux and go into the localized region.

In case of the metallic zigzag nanotubes ( $n = 3q$  where  $q$  is integer), one of the discrete value of  $k_c (= 2\pi p/na)$  intersects the K point at  $k_c = 4\pi/3a$ . The AB flux along the axis of a tube shifts the electronic state from the K point to

$$k_c(n_\Phi) = \frac{4\pi}{3a} - \frac{2\pi n_\Phi}{|\mathbf{C}_h|}, \quad (5)$$

where  $n_\Phi$  is number of the flux quantum. In the presence of a uniform magnetic field of  $B$  [T],  $n_\Phi$  for  $(n, 0)$  zigzag tube is expressed by

$$n_\Phi \equiv \frac{BS}{\Phi_0} = \frac{B}{B_1} n^2, \quad (6)$$

where  $S = \pi(na/2\pi)^2$  is the cross sectional area of the nanotube,  $\Phi_0 = 4.1 \times 10^5$  [T  $\text{\AA}^2$ ], and  $B_1 = 8.5 \times 10^5$  [T]. Thus,  $n_\Phi = 1$  (or  $\Phi_0$ ) corresponds to  $B \approx 1000$  [T] for  $n = 30$  (diameter of the tube:  $d_t = |\mathbf{C}_h|/\pi$  is 2.35 nm). 1000 [T] is beyond an accessible magnetic field. However,

the transition from an extended state to an edge state does not require such a strong magnetic field even for  $d_t \approx 2$  nm. Comparing Eq. (4) with Eq. (5), we see that the magnetic field which shifts from the K point to the critical state is proportional to  $|\mathbf{C}_h|/L$  as

$$n_{\Phi}^{\text{critical}} = \frac{|\mathbf{C}_h|}{2\pi L}, \quad \left( \text{or } L^{\text{critical}} = \frac{B_1}{B} \frac{a^2}{2\pi^2 d_t} \right). \quad (7)$$

Since  $L \gg |\mathbf{C}_h|$  holds for nanotubes, the magnetic field for the critical state becomes much smaller than 1000[T]. For example, corresponding magnetic field becomes 10[T] when  $L$  is larger than  $L^{\text{critical}} = 230$  nm for a (15,0) zigzag nanotube.

Although the critical states exist at the K' point, the critical states at the K and K' points do not occur simultaneously. It is because that the critical states at the K' point appears for  $1 - n_{\Phi}$  flux.

When the curvature effect ( $\alpha \neq 0$ ) is included, the expression for  $k_c$  (Eq. (4)) is modified. From Eq. (1), we obtain

$$k_c^{\text{critical}} \approx \frac{4\pi}{3a} - \frac{1}{L} - \frac{\alpha}{n^2 \ell}, \quad (L \gg \ell). \quad (8)$$

By comparing Eq. (4) with Eq. (8), we see that the curvature effect increases the distance between the electronic state and the critical state by  $\alpha/n^2 \ell$ . Then, comparing Eq. (8) with Eq. (5), we see that the magnetic field which shifts from the K point to the critical state becomes

$$n_{\Phi}^{\text{critical}} = \frac{|\mathbf{C}_h|}{2\pi L} + \frac{\alpha}{2\pi n} \frac{a}{\ell}, \quad \left( \text{or } L^{\text{critical}} = \frac{1}{\frac{B}{B_1} \frac{2\pi^2 d_t}{a^2} - \frac{\alpha}{\pi^2 d_t^2 \ell}} \right). \quad (9)$$

Since the  $L^{\text{critical}}$  corresponding to  $n_{\Phi}^{\text{critical}}$  becomes infinite when  $d_t = 4.2(\alpha/B[\text{T}])^{1/3}$  nm in Eq. (9),  $d_t$  must be larger than this value to reach the critical states for a finite length nanotube. For example,  $d_t$  must be larger than 1.66 nm for  $B = 20$  [T]. It is important to note that we do not need to discuss the case that the localization length  $\xi$  is larger than  $L$ . In order to observe the critical transition in experiments, it is sufficient to get  $\xi = L/2$ . By putting  $k_t = i/\xi$  with  $\xi = L/2$  to Eq. (1), we obtain

$$L^{2\xi} = \frac{2 \coth(2)}{\frac{B}{B_1} \frac{2\pi^2 d_t}{a^2} - \frac{\alpha}{\pi^2 d_t^2 \ell}}, \quad (10)$$

instead of Eq. (9). The finite localization length appears as a factor of  $2 \coth(2) \approx 2.1$ . In Fig. 2, we plot  $L^{2\xi}$  in Eq. (10) as a function of  $d$  for  $B = 20$  [T] and 40 [T] for metallic zigzag nanotubes ( $n = 3q$ ). The shaded area in Fig. 2 corresponds to possible length and diameter to observe the LD transition at  $B = 20$  [T] or lower.

In the case of semiconducting nanotubes,  $k_c$  does not exist at the K point, which requires a large  $B$  as is shown

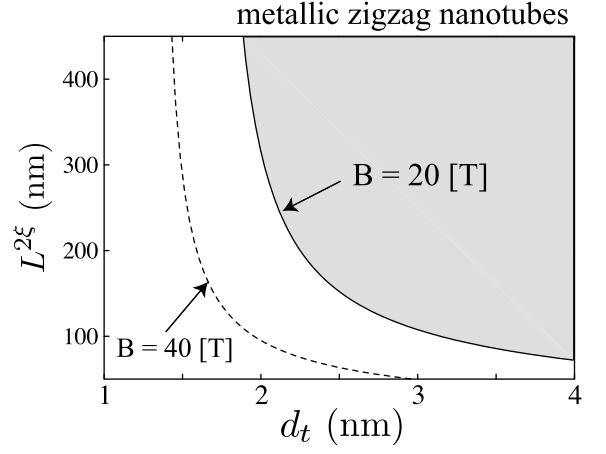


FIG. 2: The minimum length ( $L^{2\xi}$ ) and diameter ( $d_t$ ) for obtaining the critical states by AB effect for 20[T] (solid curve) and 40[T] (dashed curve). The curves diverge at  $d_t = 4.2(\alpha/B[\text{T}])^{1/3}$  nm.

below. Semiconducting zigzag nanotubes are divided into type I ( $2n = 3p + 1$ ) and type II ( $2n = 3p - 1$ ) where  $p$  is integer.<sup>23</sup> Since  $p = 2n/3 - 1/3$  holds for type I and  $p = 2n/3 + 1/3$  for type II, we have the electronic states at

$$k_c = \frac{2\pi p}{na} = \frac{4\pi}{3a} \mp \frac{2\pi}{3na}, \quad (11)$$

where minus (plus) sign in front of  $2\pi/3na$  is for type I (II). Then, in the presence of the magnetic field, we have

$$k_c = \frac{4\pi}{3a} \mp \frac{2\pi}{3na} - \frac{2\pi n_{\Phi}}{|\mathbf{C}_h|}. \quad (12)$$

The electronic states of type I which are located closest to the critical states are the edge states when  $B = 0$ , and become the extended states by applying a magnetic field (delocalization). Those for type II are the extended states when  $B = 0$ , and become the edge states by  $B$ . Comparing this with Eq. (8), we see that

$$n_{\Phi}^{\text{critical}} = \frac{|\mathbf{C}_h|}{2\pi L} + \frac{\alpha}{2\pi n} \frac{a}{\ell} \mp \frac{1}{3} \quad (13)$$

is necessary to obtain the critical states in the semiconducting nanotubes. Due to the last term ( $\mp 1/3$ ), we need a large diameter tube of order of 10 nm in order to see the critical states by an accessible magnetic field. In this respect, semiconducting tubes are not suitable to observe the critical states.

### III. CONTINUOUS MODEL

In the previous section, we have shown within the tight-binding model that the extended states are changed into the edge states through the critical states by the AB

flux. The existence of the edge states and the critical states at  $k_t = 0$  (or  $k_t = \pi/\ell$ ) is originated from the boundary condition of Eq. (1). In this section, we try to explain the LD transition using a continuous model, which is useful to understand the phenomena intuitively.

In the continuous model for nanotubes, the modification of hopping integral due to a local lattice deformation appears as a deformation-induced gauge field,  $\mathbf{A}^q(\mathbf{r})$ , in the Weyl equation,<sup>24,25</sup>  $\mathcal{H}_K\psi_K(\mathbf{r}) = E\psi_K(\mathbf{r})$  where

$$\mathcal{H}_K = v_F \boldsymbol{\sigma} \cdot (\mathbf{p} + \mathbf{A}^q(\mathbf{r})), \quad (14)$$

$v_F$  is the Fermi velocity, and  $\boldsymbol{\sigma} = (\sigma_x, \sigma_y)$  is the Pauli spin matrix. The wave function  $\psi_K(\mathbf{r}) = {}^t(\psi_A(\mathbf{r}), \psi_B(\mathbf{r}))$  has two components which represent the wave functions for two atoms (A and B) in the unit cell. As we mention in Introduction, since the two component wave function is similar to the electron spin, we call  $\psi_K(\mathbf{r})$  the pseudo-spin.  $\mathbf{A}^q(\mathbf{r})$  is different from the electro-magnetic gauge field  $\mathbf{A}^{\text{em}}(\mathbf{r})$  in the sense that the  $\mathbf{A}^q(\mathbf{r})$  holds time-reversal symmetry.<sup>25</sup> By considering a bond-cutting procedure at the edge as an extreme case of the deformation (see Fig. 3(a)), we showed that the deformation-induced “magnetic” field,  $\mathbf{B}^q(\mathbf{r}) \equiv \nabla \times \mathbf{A}^q(\mathbf{r})$ , appears at the zigzag edge (Fig. 3(b)). The  $\mathbf{B}^q(\mathbf{r})$  field represents the boundary condition for the zigzag edge (Eq. (1)) and explains the occurrence of the edge states.<sup>26</sup> Since  $\mathbf{A}^q(\mathbf{r})$  is a vector which lies on the surface of the graphene and has only  $x$ -component,<sup>26</sup>  $\mathbf{B}^q(\mathbf{r}) = (0, 0, B_z^q(\mathbf{r}))$  is normal to the nanotube surface ( $z$ -direction). The direction of  $\mathbf{B}^q(\mathbf{r})$  field becomes opposite for the both ends of a zigzag nanotube. That is, for a zigzag edge consisting of A-atoms, we have  $\mathbf{B}^q(\mathbf{r})$ , while for another zigzag edge consisting of B-atoms, we have  $-\mathbf{B}^q(\mathbf{r})$  (see Fig. 3). Since Eq. (14) does not depend on  $t$  explicitly, the energy of the system is conserved.

We consider the particle velocity,  $\mathbf{v} = (v_x, v_y)$ , defined by

$$\mathbf{v} \equiv \frac{d\mathbf{r}}{dt} = \frac{1}{i\hbar} [\mathbf{r}, \mathcal{H}_K]. \quad (15)$$

Using Eq. (14), we get  $\mathbf{v} = v_F \boldsymbol{\sigma}$ . For a Dirac particle with momentum  $\mathbf{p} (= |\mathbf{p}|\hat{\mathbf{p}})$ , we obtain  $\langle \mathbf{v} \rangle = v_F \hat{\mathbf{p}}$ . The motion of the edge states can be understood from the time-derivative of  $v_x$  and  $v_y$ :

$$\begin{aligned} \frac{dv_x}{dt} &= \frac{1}{i\hbar} [v_F \sigma_x, \mathcal{H}_K] = \frac{2v_F^2}{\hbar} \sigma_z \pi_y, \\ \frac{dv_y}{dt} &= \frac{1}{i\hbar} [v_F \sigma_y, \mathcal{H}_K] = -\frac{2v_F^2}{\hbar} \sigma_z \pi_x, \end{aligned} \quad (16)$$

where  $\boldsymbol{\pi} = (\pi_x, \pi_y) (\equiv \mathbf{p} + \mathbf{A}^q(\mathbf{r}))$  is the kinematical momentum. The wave function of the edge state ( $\psi^{\text{edge}}(\mathbf{r})$ ) is polarized in terms of the pseudo-spin. In fact,  $\psi_K^{\text{edge}}(\mathbf{r}) \propto {}^t(1, 0)$  near the zigzag edge consisting of A-atoms and  $\psi_K^{\text{edge}}(\mathbf{r}) \propto {}^t(0, 1)$  near the zigzag edge consisting of B-atoms. We have  $\langle \sigma_z \rangle = \pm 1$  for pseudo-spin polarized states. Then, by putting  $\mathbf{r} = r^{\text{cyc}}(\sin \omega t, \cos \omega t)$

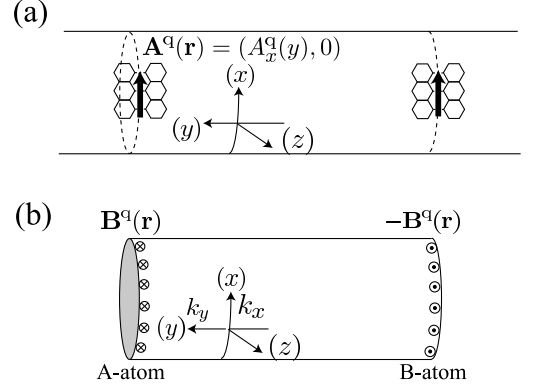


FIG. 3: (a) A zigzag nanotube is obtained from a periodic tube by cutting the bonds at the zigzag edge. The change of the hopping integral due to the bond-cutting appears as the deformation-induced gauge field,  $\mathbf{A}^q(\mathbf{r})$ , in the Weyl equation. (b) The deformation-induced “magnetic” field  $\mathbf{B}^q(\mathbf{r})$  appears at the zigzag edge. For a zigzag edge consisting of A-atoms,  $\mathbf{B}^q(\mathbf{r})$  points to the negative  $z$ -direction, while it is positive direction for a zigzag edge consisting of B-atoms.  $\mathbf{B}^q(\mathbf{r})$  does not depend on  $x$  due to the translational symmetry.

and  $\mathbf{p} = |\mathbf{p}|(\cos \omega t, -\sin \omega t)$  into  $\langle d\mathbf{r}/dt \rangle = v_F \hat{\mathbf{p}}$  and Eq. (16), we get the cyclotron motion with the cyclotron radius,  $r^{\text{cyc}} = 2\hbar/|\mathbf{p}|$  in the absence of  $\mathbf{A}^q(\mathbf{r})$  field. Since only the  $x$ -component of the  $\mathbf{A}^q(\mathbf{r})$  field appears at the zigzag boundary ( $y = 0$ ),<sup>26</sup> we have  $\pi_x = p_x + A_x^q(y)$  and  $\pi_y = p_y$ . Thus, for the initial pseudo-spin polarized state with  $p_y = 0$ , the state follows the cyclotron motion and  $v_y$  changes the sign at the boundary due to  $A_x^q(y)$  as shown in Fig. 4(b). The corresponding states are the edge states. In fact, the localization length of the edge states is calculated as  $\xi = \hbar/|p_x|$  in the continuous model,<sup>26</sup> which is the same as the  $r^{\text{cyc}}/2$  for  $p_y = 0$ . The cyclotron motion of the edge state is the eigenstate of the total angular momentum ( $J_z = \hat{\mathbf{z}} \cdot (\mathbf{r} \times \boldsymbol{\pi}) + (\hbar/2)\sigma_z$ ) with eigenvalue  $J_z = \mp 3\hbar/2$ .

To see the correspondence more in detail, we need to consider how the pseudo-spin polarization is achieved by the  $\mathbf{A}^q(\mathbf{r})$  field. Time-evolution of the  $\sigma_z$  is given by

$$\frac{d\sigma_z}{dt} = \frac{1}{i\hbar} [\sigma_z, \mathcal{H}_K] = \frac{2v_F}{\hbar} \boldsymbol{\sigma} \cdot (\hat{\mathbf{z}} \times \boldsymbol{\pi}). \quad (17)$$

In the absence of  $\mathbf{A}^q(\mathbf{r})$ , since  $\boldsymbol{\sigma}$  and  $\mathbf{p}$  are parallel or anti-parallel for the extended states (helicity),<sup>27</sup> we have  $\langle \sigma_z \rangle = 0$  and  $\langle d\sigma_z/dt \rangle = 0$ , and Eq. (16) does not give the cyclotron motion. On the other hand, at the zigzag edge,  $d\sigma_z/dt \neq 0$  since  $\mathbf{A}^q(\mathbf{r}) \neq 0$ . Moreover, it can be shown that  $d^2\sigma_z/dt^2 = -4\sigma_z(\mathcal{H}_K/\hbar)^2 + (2v_F^2/\hbar)\hat{\mathbf{z}} \cdot \mathbf{B}^q(\mathbf{r})$ . Thus, the pseudo-spin (or the edge states) is accumulated at the zigzag edge.

The scattering process at the zigzag edge for the extended (pseudo-spin unpolarized,  $\langle \sigma_z \rangle = 0$ ) states can be understood by the equation of motion of  $\boldsymbol{\pi}$ , which is

given by

$$\frac{d\boldsymbol{\pi}}{dt} = \frac{1}{i\hbar} [\boldsymbol{\pi}, \mathcal{H}_K] = -v_F \boldsymbol{\sigma} \times \mathbf{B}^q(\mathbf{r}). \quad (18)$$

The right-hand side of Eq. (18) shows that the Dirac particle undergoes a ‘‘Lorentz force’’:

$$\mathbf{f}(\mathbf{r}) = -\mathbf{v} \times \mathbf{B}^q(\mathbf{r}). \quad (19)$$

The Lorentz force rotates the momentum  $\mathbf{p}$  of the incident Dirac particle at the zigzag boundary. Due to the helicity conservation, the pseudo-spin and  $\mathbf{p}$  are parallel ( $\langle \mathbf{v} \rangle = v_F \hat{\mathbf{p}}$ ) in the scattering process. We consider the time-evolution of the following four initial states specified by  $\mathbf{v} = (v_x, v_y)$  as (1) ( $v_x > 0, v_y > 0$ ), (2) ( $0, v_y > 0$ ), (3) ( $v_x < 0, v_y > 0$ ), and (4) ( $0, 0$ ). The corresponding position of each initial state in the  $k$ -space is shown in Fig. 4(a). Hereafter, we denote the  $(x, y)$  components of  $\mathbf{f}$  as  $(f_x, f_y)$ .

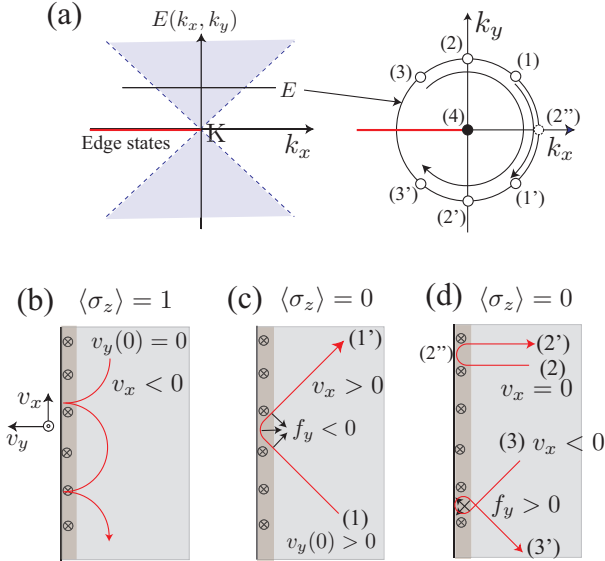


FIG. 4: (color online) (a) We consider the scattering processes for the initial states at (1)~(3) in the  $k$ -space with energy  $E \neq 0$ , and the initial state at (4) with  $E = 0$ . (b) The motion of the edge state is the cyclotron motion. (c,d) The velocity  $\mathbf{v} = (v_x, v_y)$  causes the Lorentz force,  $-\mathbf{v} \times \mathbf{B}^q(\mathbf{r})$ , at the edge sites. The force can attract or reflect an incident electron depending on the sign of  $v_x$ .

First, we consider the scattering process for (1). When  $v_x > 0$ , we have  $f_y < 0$  from Eq. (19) and  $\mathbf{B}^q(\mathbf{r})$  field reflects the electron at the zigzag edge. The trajectory of the Dirac particle is shown in Fig. 4(c), and the final state is given by (1'). Due to the energy conservation, the time-evolution of  $\mathbf{p}$  is restricted on the circle with radius  $|\mathbf{p}|$  in the  $k$ -space.

Next, we consider the initial state of (2) (see Fig. 4(d)). In this case, the state is reflected by the zigzag edge and changes the sign of  $v_y$ , and the final state is given by

(2'). The time-evolution of the  $\mathbf{v}$  in this scattering process is as follows. First, the  $\mathbf{B}^q(\mathbf{r})$  field changes  $(0, v_y)$  to  $(f_x dt, 0)$  ((2'')) in Fig. 4(a)) in a very short period ( $dt$ ). Then, the velocity of the virtual state is rotated by  $\mathbf{B}^q(\mathbf{r})$  field again, and the final state becomes  $(0, -v_y)$ . This explains that the state moves in the clockwise direction in the  $k$ -space (see Fig. 4(a)) and reaches the final state. The presence of  $\mathbf{B}^q(\mathbf{r})$  field gives rise to a phase shift in the scattering process, and yields the backward scattering. According to the absence of the backward scattering mechanism,<sup>28</sup> the Berry's phase shift of  $\pi$  between the two scattered waves corresponding to the clockwise and anticlockwise rotation in the  $k$ -space, cancels the back-scattering amplitude. The  $\mathbf{B}^q(\mathbf{r})$  field selects only the clockwise motion in the  $k$ -space and recovers the backward scattering at the zigzag edge.

For the initial state of (3), the direction of  $f_y$  becomes  $f_y > 0$  and then the  $\mathbf{B}^q(\mathbf{r})$  field tends to trap the electrons. However, due to the energy conservation, the electron can escape from the edge and the final state is given by (3'). The trajectory of the Dirac particle is shown in Fig. 4(d).

Finally, for the initial state of (4) (i.e., particle at the Dirac point), the particle is not affected by  $\mathbf{B}^q(\mathbf{r})$  field ( $\mathbf{f} = \mathbf{0}$ ). The AB flux along the axis of a tube gives a finite  $v_x$  and the  $\mathbf{B}^q(\mathbf{r})$  field produces the non-vanishing Lorentz force. Then, the  $\mathbf{B}^q(\mathbf{r})$  field attracts the state with  $v_y = 0$  at the zigzag edge if  $v_x < 0$ . The state at the Dirac point is unstable against the AB flux and undergoes the LD transition. This state is nothing but the critical state that we discussed in this paper.

#### IV. DISCUSSION

It is interesting that the localization phenomena discussed in this paper is analogous to the spin Hall effect (SHE).<sup>20,21,22</sup> In the SHE, the spin current is accumulated near the edges of semiconductor materials by the electric field applied along the edge. Since the time derivative of the AB flux gives an electronic field along the zigzag edge, the physical situation discussed in this paper is similar to that of the SHE. The wave function of the edge state in graphene is polarized in terms of the pseudo-spin. Since the extended state is a pseudo-spin unpolarized state, the pseudo-spin is accumulated by the localization. Thus, by neglecting the difference between the (real) spin in the SHE and the pseudo-spin, the situations of these systems are quite similar to each other.

Moreover, the spin edge states accumulated by the SHE can be understood in the case of the Rashba spin-orbit Hamiltonian,<sup>21</sup> by the deformation-induced gauge field, too. The spin-orbit Hamiltonian in the SHE is given by

$$\mathcal{H}_{so} = -\frac{\lambda}{\hbar} \boldsymbol{\sigma} \cdot (\hat{\mathbf{z}} \times \mathbf{p}), \quad (20)$$

where  $\lambda$  is the Rashba coupling constant and  $\hat{\mathbf{z}}$  is the unit

TABLE I: Analogy between graphene and SHE

	Graphene	SHE
Wave function	Pseudo-spin	Spin
Hamiltonian	$\mathcal{H}_K = v_F \boldsymbol{\sigma} \cdot \boldsymbol{\pi}$	$\mathcal{H}_{so} = -(\lambda/\hbar) \boldsymbol{\sigma} \cdot (\hat{\mathbf{z}} \times \mathbf{p})$
$d\sigma_z/dt$	$(2v_F/\hbar) \boldsymbol{\sigma} \cdot (\hat{\mathbf{z}} \times \boldsymbol{\pi})$	$(2\lambda/\hbar^2) \boldsymbol{\sigma} \cdot \mathbf{p}$
$d^2\sigma_z/dt^2$	$-4\sigma_z(\mathcal{H}_K/\hbar)^2 + (2v_F^2/\hbar) B_z^q(\mathbf{r})$	$-4\sigma_z(\mathcal{H}_{so}/\hbar)^2$

vector perpendicular to the plane. First, we assume that the system is a cylindrical shape and periodic about  $y$  direction. Then we introduce the boundary at  $y = 0$  by replacing  $p_x$  with  $p_x - \text{sign}(p_x) A_x^q(y)$  in Eq. (20) where  $A_x^q(y) (> 0)$  is non-vanishing near the boundary  $-\xi_g < y < \xi_g$  and  $\text{sign}(p_x)$  keeps the time-reversal symmetry. The localized energy eigenstates can be obtained as<sup>26</sup>

$$\psi_E(\mathbf{r}) = \begin{cases} \exp\left(i\frac{p_x x}{\hbar}\right) e^{-y/\xi} \begin{pmatrix} 1 \\ 0 \end{pmatrix} & (y > 0) \\ \exp\left(i\frac{p_x x}{\hbar}\right) e^{-y/\xi} \begin{pmatrix} 0 \\ i \end{pmatrix} & (y < 0), \end{cases} \quad (21)$$

where

$$\frac{\hbar}{\xi} = p_x \tanh\left(\frac{\text{sign}(p_x)}{\hbar} \int_{-\xi_g}^{\xi_g} A_x^q(y) dy\right). \quad (22)$$

Thus, by applying the electric field along  $x$ -direction, the initial extended state with  $p_x = 0$  ( $\xi = \infty$ ) becomes  $p_x \neq 0$  due to  $dp_x/dt = -eE$ , and can be localized. This state can be considered as the critical state in the SHE. The analogy between graphene and SHE systems is summarized in Table I. It is interesting to see that the Hamiltonian and time-evolution for polarization for graphene and SHE have a special dual symmetry.

Albeit the similarity between the SHE and our system, there are several differences. First, by increasing the AB flux continuously to give a constant electronic field, the delocalization process occurs at the K' point. It means that the pseudo-spin at the edge is not always increasing. Second, the localization phenomena in our system depends on the shape of the edge, while such the structure dependent spin accumulation is not known for the SHE. In our system, the dependence of the localization on the shape of the edge is given by  $\mathbf{B}^q(\mathbf{r})$  field.<sup>26</sup> To clarify this point, it is necessary to derive the deformation-induced gauge field for the SHE ( $A_x^q(y)$  in Eq. (22)) from a microscopic lattice model, which will be reported elsewhere.

The pseudo-spin accumulation may be useful like the applications for the SHE since the presence of the edge states is predicted to make the ferromagnetism in the presence of the Coulomb interaction.<sup>4</sup> Moreover, the electron-phonon interaction for the pseudo-spin polarized states is stronger than that for the extended states. The strong electron-phonon interaction may give rise to the superconducting states of the edge states.<sup>5</sup> Thus, we think that the coexistence of the localization transition described by the pseudo-spin accumulation and real-spin polarization by Coulomb interaction will be an important subject of physics.

It is known that the next nearest-neighbor (nnn) hopping process gives a finite energy bandwidth for the edge states.<sup>29</sup> Since the nnn hopping breaks the particle-hole symmetry, the shift of the energy for the critical state becomes either positive or negative value depending on the conduction or valence critical state, respectively. Denoting the nnn hopping integral  $\gamma_n$ , the shift of the critical state is given by adding  $\pm c/L$  in Eq. (8) with  $c \approx \gamma_n/\gamma_0$ . Theoretically,  $c$  can be estimated around 0.1 by Porezag *et al.*<sup>30</sup> Since  $\gamma_n$  is renormalized by the electron-phonon interaction,  $c$  becomes much smaller than 0.1.<sup>31</sup> Thus, the change of  $L$  in Eq. (10) due to  $\gamma_n$  is less than 10 % and is negligible.

In conclusion, we have shown that AB flux around 20[T] induces localization-delocalization transition for the edge states for metallic zigzag carbon nanotubes. The localization is similar to the spin accumulation by the SHE when we regard the pseudo-spin as the electron spin. The LD transition can be observed by means of STM/STS.

## Acknowledgments

The authors would like to thank S. Murakami for valuable comments.

\* Email address: sasaken@flex.phys.tohoku.ac.jp

<sup>1</sup> K. S. Novoselov, A. K. Geim, S. V. Morozov, D. Jiang, M. I. Katsnelson, I. V. Grigorieva, S. V. Dubonos, and A. A. Firsov, *Nature* **438**, 197 (2005).

<sup>2</sup> Y. Zhang, Y.-W. Tan, H. L. Stormer, and P. Kim, *Nature*

**438**, 201 (2005).

<sup>3</sup> H. B. Heersche, P. Jarillo-Herrero, J. B. Oostinga, L. M. K. Vandersypen, and A. F. Morpurgo, *Nature* **446**, 56 (2007).

<sup>4</sup> M. Fujita, K. Wakabayashi, K. Nakada, and K. Kusakabe, *J. Phys. Soc. Jpn.* **65**, 1920 (1996).

- <sup>5</sup> K. Sasaki, J. Jiang, R. Saito, S. Onari, and Y. Tanaka, J. Phys. Soc. Jpn. **76**, 033702 (2007).
- <sup>6</sup> H. Ajiki and T. Ando, J. Phys. Soc. Jpn. **62**, 2470 (1993).
- <sup>7</sup> K. Sasaki, S. Murakami, R. Saito, and Y. Kawazoe, Phys. Rev. B **71**, 195401 (2005).
- <sup>8</sup> Y. Niimi, T. Matsui, H. Kambara, K. Tagami, M. Tsukada, and H. Fukuyama, Appl. Surf. Sci. **241**, 43 (2005).
- <sup>9</sup> Y. Kobayashi, K. Fukui, T. Enoki, K. Kusakabe, and Y. Kaburagi, Phys. Rev. B **71**, 193406 (2005).
- <sup>10</sup> P. L. Giunta and S. P. Kelty, The Journal of Chemical Physics **114**, 1807 (2001).
- <sup>11</sup> Z. Klusek, Z. Waqar, E. A. Denisov, T. N. Kompaniets, I. V. Makarenko, A. N. Titkov, , and A. S. Bhatti, Appl. Surf. Sci. **161**, 508 (2000).
- <sup>12</sup> Y. Niimi, T. Matsui, H. Kambara, K. Tagami, M. Tsukada, and H. Fukuyama, Phys. Rev. B **73**, 085421 (2006).
- <sup>13</sup> Y. Kobayashi, K. Fukui, T. Enoki, and K. Kusakabe, Phys. Rev. B **73**, 125415 (2006).
- <sup>14</sup> A. Bachtold, C. Strunk, J.-P. Salvetat, J.-M. Bonard, L. Forr, T. Nussbaumer, and C. Schönenberger, Nature **397**, 673 (1999).
- <sup>15</sup> U. C. Coskun, T.-C. Wei, S. Vishveshwara, P. M. Goldbart, and A. Bezryadin, Science **304**, 1132 (2004).
- <sup>16</sup> S. Roche, G. Dresselhaus, M. S. Dresselhaus, and R. Saito, Phys. Rev. B **62**, 16092 (2000).
- <sup>17</sup> R. Saito, G. Dresselhaus, and M. S. Dresselhaus, Phys. Rev. B **61**, 2981 (2000).
- <sup>18</sup> S. Zaric, G. N. Ostojic, J. Kono, J. Shaver, V. C. Moore, M. S. Strano, R. H. Hauge, R. E. Smalley, and X. Wei, Science **304**, 1129 (2004).
- <sup>19</sup> E. D. Minot, Y. Yaish, V. Sazonova, and P. L. McEuen, Nature **428**, 536 (2004).
- <sup>20</sup> S. Murakami, N. Nagaosa, and S.-C. Zhang, Science **301**, 1348 (2003).
- <sup>21</sup> J. Sinova, D. Culcer, Q. Niu, N. A. Sinitsyn, T. Jungwirth, and A. H. MacDonald, Phys. Rev. Lett. **92**, 126603 (2004).
- <sup>22</sup> J. E. Hirsch, Phys. Rev. Lett. **83**, 1834 (1999).
- <sup>23</sup> R. Saito, K. Sato, Y. Oyama, J. Jiang, G. G. Samsonidze, G. Dresselhaus, and M. S. Dresselhaus, Phys. Rev. B **72**, 153413 (2005).
- <sup>24</sup> C. L. Kane and E. J. Mele, Phys. Rev. Lett. **78**, 1932 (1997).
- <sup>25</sup> K. Sasaki, Y. Kawazoe, and R. Saito, Prog. Theo. Phys. **113**, 463 (2005).
- <sup>26</sup> K. Sasaki, S. Murakami, and R. Saito, J. Phys. Soc. Jpn. **75**, 74713 (2006).
- <sup>27</sup> T. Ando, J. Phys. Soc. Jpn. **74**, 777 (2005).
- <sup>28</sup> T. Ando, T. Nakanishi, and R. Saito, J. Phys. Soc. Jpn. **67**, 2857 (1998).
- <sup>29</sup> K. Sasaki, S. Murakami, and R. Saito, Applied Physics Letters **88**, 113110 (2006).
- <sup>30</sup> D. Porezag, T. Frauenheim, T. Köhler, G. Seifert, and R. Kaschner, Phys. Rev. B **51**, 12947 (1995).
- <sup>31</sup> K. Sasaki, K. Sato, R. Saito, J. Jiang, S. Onari, and Y. Tanaka, Phys. Rev. B **75**, 235430 (2007).